ADVANCED MATERIALS
www.advmat.de

Materials Views
www.MaterialsViews.com

Exceptional Superionic Conductivity in Disordered Sodium Decahydro-*closo*-decaborate

Terrence J. Udovic, Motoaki Matsuo, Wan Si Tang, Hui Wu, Vitalie Stavila, Alexei V. Soloninin, Roman V. Skoryunov, Olga A. Babanova, Alexander V. Skripov, John J. Rush, Atsushi Unemoto, Hitoshi Takamura, and Shin-ichi Orimo**

Recently, complex hydride salts undergoing solid-state, entropy-driven, order–disorder transitions have been shown to exhibit impressive fast-ion conduction properties as a result of the appearance of vacancy-rich cation sublattices within networks of highly mobile, reorientationally disordered polyanions.[1] Initial interest has mainly focused on the light-metal Li and Na salts possessing tetrahydroborate (BH_4^-) polyanions (see **Figure 1**), such as $LiBH_4$ and $Na_2BH_4NH_2$, as well as related derivative materials.[2–5] Very recently, it was discovered that Li and Na salts possessing the larger icosahedral dodecahydro-*closo*-dodecaborate ($B_{12}H_{12}^{2-}$) anions (see Figure 1) also undergo order–disorder phase transitions,[6,7] with $Na_2B_{12}H_{12}$ exhibiting disorder-induced superionic conductivity (approaching 0.1 S cm^{-1}) above around 480 K.[8] This conductivity rivals that of traditional ceramic materials, Na β"-alumina solid electrolyte (BASE), and Na superionic conductor (NASICON), as well as more recent Na_3PS_4-based glass ceramic electrolytes, all currently of considerable interest for use in Na-ion batteries.[9–11] The pronounced superionicity and relatively low conduction barrier for disordered $Na_2B_{12}H_{12}$ are probably due, in part, to the larger size (and roughly spherical shape) of the $B_{12}H_{12}^{2-}$ anions compared with the substantially smaller BH_4^- anions (see Figure 1) present in other investigated fast-ion conductors.[1] These types of large polyanion compounds represent a potentially fertile area for discovering new materials with superionic conductivities, but with lower transition temperatures. Here we report our finding that sodium decahydro-*closo*-decaborate ($Na_2B_{10}H_{10}$), a related sodium salt containing large, ellipsoidal-shaped, $B_{10}H_{10}^{2-}$ anions (see Figure 1), forms a disordered, face-centered-cubic (fcc) phase above ca. 360 K, possessing a vacancy-rich Na^+ cation sublattice. This cation sublattice is highly mobile within the spacious corridors formed by the large $B_{10}H_{10}^{2-}$ anions and exhibits remarkable superionic conductivity (e.g., $\sigma \approx 0.01$ S cm^{-1} at 383 K) to substantially lower temperatures than for $Na_2B_{12}H_{12}$. This conductivity is more than an order of magnitude higher than that of all other solid-state Na-based complex-hydride materials investigated to date in this temperature region.[1] As such, this discovery represents a major advancement in the field of solid-state Na^+ fast-ion conduction at technologically relevant device temperatures.

Figure 2 shows differential scanning calorimetry (DSC) results for $Na_2B_{10}H_{10}$ after several heating/cooling cycles. There is a clear reversible transition, first observed by Bonnetot et al.,[12] with minor hysteresis. After a number of cycles to 500 K, the hysteresis decreases and the onset temperature stabilizes near 360 K upon both heating and cooling. A slow attenuation of the DSC features begins to occur upon repeated cycling to temperatures near 600 K.

Figure 3 shows the neutron powder diffraction (NPD) result for a partially deuterated $Na_2{}^{11}B_{10}H_{10}$ sample at 410 K, above the phase transition. Table S1 in the Supporting Information lists the corresponding structural parameters. The Rietveld-refined model confirms transformation from the known, low-*T*, ordered monoclinic structure[13] (not shown) to a high-*T* disordered structure with Na^+ cations partially occupying a variety of interstitial sites within an fcc lattice of orientationally disordered anions. Neutron-scattering Fourier difference maps initially suggested that the broad distribution of cation positions and the inclusion of the three most intense positions were ultimately necessary to attain a good model fit to the data. Furthermore, the refinements suggested extensive anion orientational disorder, which could be represented in various ways via multiple B and H positions. The model reflects the simplest

Dr. T. J. Udovic, Dr. W. S. Tang, Dr. H. Wu, Dr. J. J. Rush
NIST Center for Neutron Research
National Institute of Standards and Technology
Gaithersburg, MD 20899–6102, USA
E-mail: udovic@nist.gov

Dr. M. Matsuo, Prof. S. Orimo
Institute for Materials Research
Tohoku University
Sendai 980–8577, Japan
E-mail: orimo@imr.tohoku.ac.jp

Dr. W. S. Tang, Dr. H. Wu, Dr. J. J. Rush
Department of Materials Science and Engineering
University of Maryland
College Park, MD 20742–2115, USA

Dr. V. Stavila
Sandia National Laboratories
Livermore, CA 94551, USA

Dr. A. V. Soloninin, R. V. Skoryunov,
Dr. O. A. Babanova, Dr. A. V. Skripov
Institute of Metal Physics
Ural Branch of the Russian Academy of Sciences
Ekaterinburg 620990, Russia

Dr. A. Unemoto, Prof. S. Orimo
WPI-Advanced Institute for Materials Research
Tohoku University
Sendai 980–8577, Japan

Prof. H. Takamura
Graduate School of Engineering
Tohoku University
Sendai 980–8579, Japan

DOI: 10.1002/adma.201403157

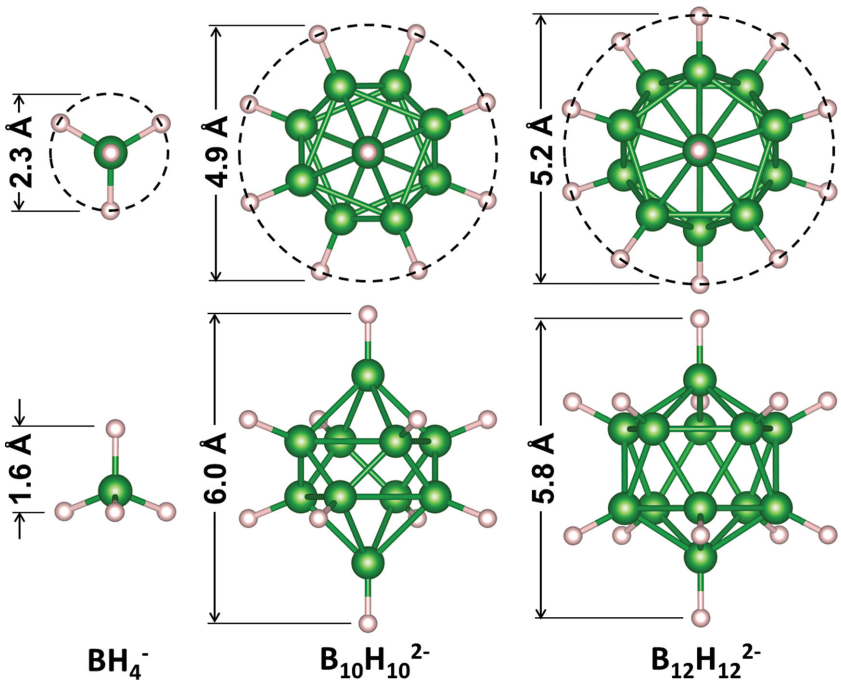

Figure 1. Geometries and approximate relative sizes of BH_4^-, $B_{10}H_{10}^{2-}$, and $B_{12}H_{12}^{2-}$ anions, each shown from top and side views. The boron and hydrogen atoms are denoted by the green and pink spheres, respectively.

representation of six approximately superimposed anion orientations, each equally probable. In particular, the six possible anion orientations are aligned in pairs with their long axes oriented along any one of the three orthogonal crystallographic axes. The members of each pair are azimuthally offset from each other by 45° about their long axes. Each B and H position in the structure is 1/3 occupied, being shared by two of the six possible orientations.

Anion dynamical behavior was probed by neutron elastic-scattering fixed-window scans (FWSs)[14] of $Na_2{}^{11}B_{10}H_{10}$. The results in **Figure 4** suggest that a dramatic change in $B_{10}H_{10}^{2-}$ anion reorientational mobility occurs upon phase transformation. In particular, the high elastic neutron counts in the low-T ordered phase suggest anion reorientational jump frequencies less than 10^8 s^{-1}, whereas the roughly 80% lower counts in the high-T disordered phase suggest an orders-of-magnitude enhancement in jump frequencies to greater than 10^{10} s^{-1}. This is reminiscent of the FWS behavior observed for $Na_2B_{12}H_{12}$.[7,15] Indeed, the inset in Figure 4 showing a quasielastic neutron scattering (QENS) spectrum for the disordered phase at 375 K indicates a quasielastic component with a Lorentzian linewidth of about 41(1) μeV FWHM, which reflects a jump correlation frequency on the order of 3×10^{10} s^{-1}. The ratio of elastic and total scattering intensities (which is also consistent with the ratio of FWS neutron counts in the disordered and ordered phases from Figure 4) suggests that, besides the $B_{10}H_{10}^{2-}$ reorientational jumps around the long axis, two-fold anion flips leading to exchanges of apical H atom positions are also occurring.

We also probed the Na^+ dynamical behavior in $Na_2B_{10}H_{10}$ by ^{23}Na NMR measurements. **Figure 5** shows the ^{23}Na spin-lattice relaxation rate R_1 at the resonance frequency of $\omega/2\pi = 23$ MHz as a function of T^{-1}. The general features of the behavior of R_1 for $Na_2B_{10}H_{10}$ resemble those for $Na_2B_{12}H_{12}$ at the phase transition.[16] Here, R_1 exhibits a jump accompanied by a change in sign of its temperature dependence. Such behavior indicates that the transition from the ordered to

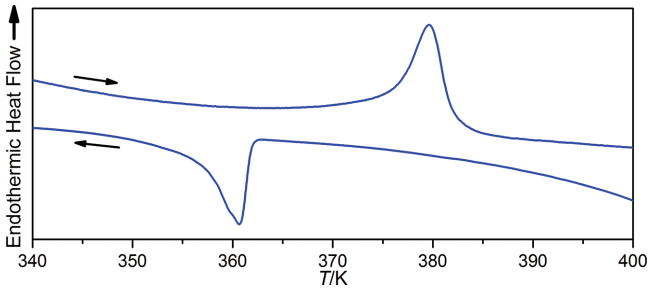

Figure 2. Characteristic DSC measurements (2 K min^{-1}) for $Na_2B_{10}H_{10}$ after several heating and cooling cycles up to 410 K.

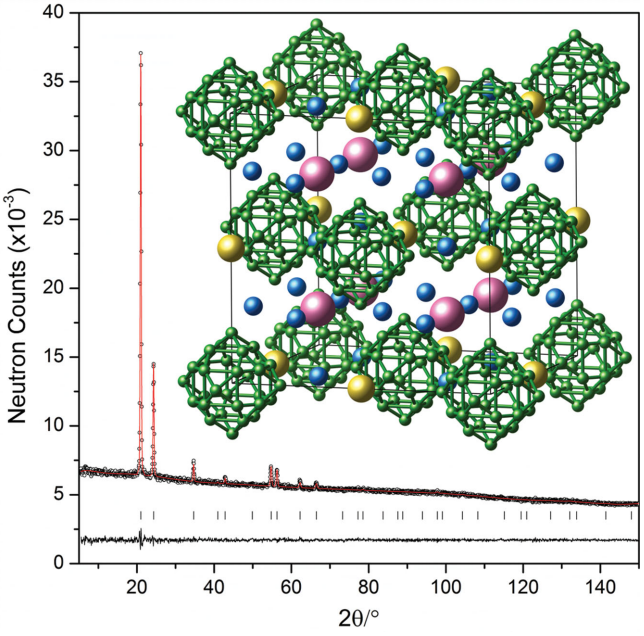

Figure 3. Experimental (circles), fitted (line), and difference (lower line) NPD profiles for $Na_2{}^{11}B_{10}(H_{0.73}D_{0.27})_{10}$ at 410K (λ = 2.077 Å; *Fm-3m*; a = 9.8426(8) Å; R_{wp} = 0.0123; R_p = 0.0104; χ^2 = 0.817). The vertical bars indicate the calculated positions of the Bragg peaks. Inset: Disordered structure. H atoms are omitted for clarity. B atoms are denoted by the green spheres. Anions are centered at *4a* (0 0 0). Different Na^+ cation positions are denoted by the red [tetrahedral (t) sites at *8c* (¼ ¼ ¼)], yellow [octahedral (o) sites at *4b* (½ 0 0)], and blue [intermediate (i) sites at *24d* (¼ ¼ 0) between two t sites] spheres. The sphere sizes are proportional to the partial occupancies of 0.58(1), 0.28(3), and 0.09(1) for the t, o, and i sites, respectively.

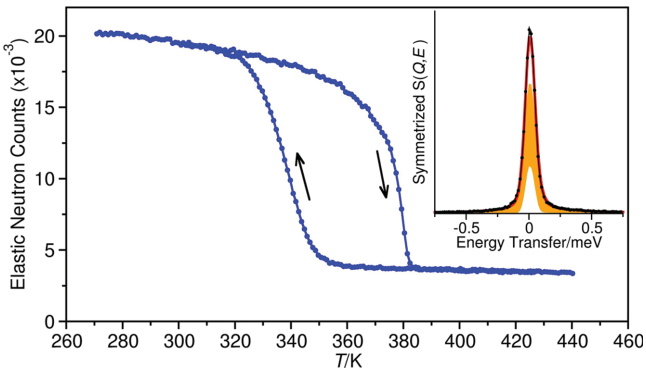

Figure 4. Neutron elastic-scattering fixed-window scan at 0.8 μeV (FWHM) instrumental resolution for $Na_2{}^{11}B_{10}H_{10}$ upon heating and cooling at 0.25 K min^{-1}, at a neutron momentum transfer Q of 0.87 Å^{-1}. The inset shows a quasielastic scattering spectrum at 375 K at the same Q value, at 79 μeV (FWHM) instrumental resolution. The fit (red) to the data (black) is composed of elastic (white) and quasielastic (orange) contributions.

the disordered phase is accompanied by an abrupt increase in the Na^+ jump rate τ_d^{-1}. The expected $R_1(T)$ maximum is 'folded'; i.e., because of the abrupt increase in τ_d^{-1} at the phase transition, there is a jump directly from the low-T slope to the high-T slope of the $R_1(T)$ peak. On the low-T slope, R_1 is proportional to τ_d^{-1}; on the high-T slope, R_1 is proportional to τ_d. From the two slopes, we obtain activation energies for Na^+ jumps in the ordered and disordered phases of 750(20) meV and 190(10) meV, respectively. Although we cannot reliably determine the absolute values of τ_d^{-1} due to the 'folded' nature of the $R_1(T)$ peak, the data do allow us to conclude that the Na^+ jump rate exceeds $\omega \approx 1.5 \times 10^8$ s^{-1} just above the phase transition. Moreover, the very small ^{23}Na NMR linewidth (0.2 kHz full-width half-maximum (FWHM)) observed in the disordered phase confirms that the Na^+ cations are undergoing long-range diffusion.

To characterize the $Na_2B_{10}H_{10}$ conduction behavior, we carried out AC impedance measurements between 295 K and 423 K using a pressed disk of polycrystalline $Na_2B_{10}H_{10}$ powder with either gold or (similarly performing) molybdenum foil contacts. Cross-sectional SEM images of the pelletized sample in Figure S1 of the Supporting Information confirm that intimate

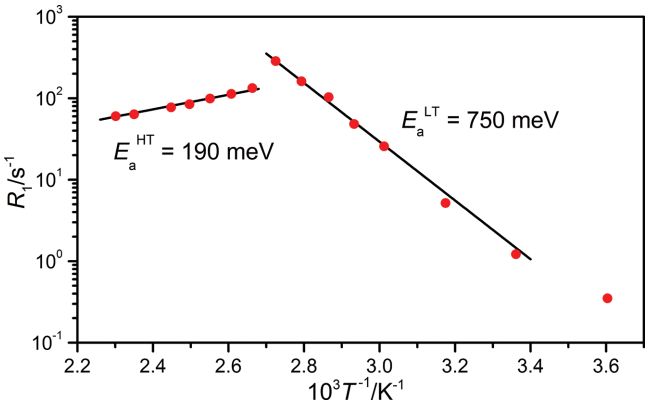

Figure 5. The ^{23}Na spin-lattice relaxation rate R_1 versus T^{-1} for $Na_2B_{10}H_{10}$ measured at 23 MHz. The solid lines show Arrhenius fits to the data for the ordered and disordered phases.

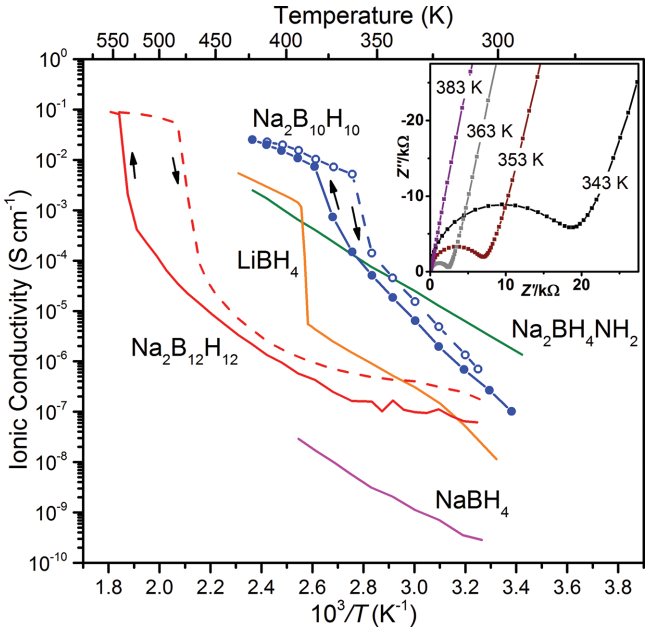

Figure 6. T-dependent ionic conductivity of $Na_2B_{10}H_{10}$ compared with that for other related materials: $Na_2B_{12}H_{12}$,[8] $Na_2BH_4NH_2$,[4] $NaBH_4$,[4] and $LiBH_4$.[2] Inset: Complex impedance plots of $Na_2B_{10}H_{10}$ measured at various temperatures during heating.

contacts among the particles were achieved. $Na_2B_{10}H_{10}$ can be easily pelletized without further sintering, as has been reported for $LiBH_4$ and other complex hydrides.[1,5] The results are shown in **Figure 6** for the gold contacts. The inset shows typical complex impedance plots at various temperatures. They consist of an arc in the high-frequency region and a spike in the low-frequency region due to contributions from the bulk/grain boundaries and the electrode, respectively. The results suggest that $Na_2B_{10}H_{10}$, similar to $Na_2B_{12}H_{12}$,[8] behaves like a typical ionic conductor. The temperature dependence of the conductivity indicates dramatic superionic conductivity above the hysteretic order–disorder transition near 373 K, rising two orders of magnitude higher than that in the low-T phase. This behavior is superior to that of other investigated complex hydride materials. Indeed, the conductivity exhibits a value of about 0.01 S cm^{-1} at 383 K, which is about 25× greater than that of $Na_2BH_4NH_2$ (4×10^{-4} S cm^{-1}).[4] A conductivity above 0.1 S cm^{-1} at 500 K is suggested by extrapolation of the lower-T data. The activation energy for conduction is evaluated to be 0.47 eV, which is higher than that reported for $Na_2B_{12}H_{12}$ (0.21 eV)[8] but lower than those reported for $Na_2BH_4NH_2$ (0.61 eV)[4,8] and the high-T phase of $LiBH_4$ (0.53 eV).[2] Nevertheless, any rationalization of the differences based solely on anion size is complicated by the substantial differences in structure and conduction pathways.

It should be noted that the NMR-derived activation energies discussed above reflect the average microscopic barriers for all cation diffusional jumps between neighboring sites within the $Na_2B_{10}H_{10}$ lattice, some of which may have little effect on the macroscopic conductivity barrier. In contrast, the latter barrier is more reflective of an overall rate-limiting step, such as a particular type of cation jump within the material required to

maintain conduction pathways or cation transport, e.g., across grain boundaries (although such grain-boundary bottlenecks are believed to be small in the present system).

The superionic conductivity of disordered $Na_2B_{10}H_{10}$ is consistent with the relatively small activation energy for Na^+ diffusion within the liquid-like cation sublattice. Again, similar to disordered $Na_2B_{12}H_{12}$,[8] the overly large size and spheroidal shape of the polyanions result in less restrictive interstitial pathways and, hence, reduced Na^+ diffusional bottlenecks between the various cation sites within the close-packed anion sublattice.

As for the other disordered complex hydrides, the reorientationally mobile anions associated with superionic $Na_2B_{10}H_{10}$ may also lower the cation diffusional barrier by providing a dynamically cooperative environment for cation jumps within the voids of the anion sublattice. Indeed, at least an order-of-magnitude-higher anion reorientational jump rate compared with the Na^+ diffusional jump rate provides a dynamic environment where the anions can behave as 'lubricants' for cation diffusive motions.

A comparison of the relative sizes of the $B_{10}H_{10}^{2-}$ and $B_{12}H_{12}^{2-}$ anions in Figure 1 indicates a similar maximum dimension for each anion. In fact, the lattice constants for the disordered fcc $Na_2B_{10}H_{10}$ and body-centered cubic (bcc) $Na_2B_{12}H_{12}$ structures[7] indicate that both disordered anions possess similar spherical packing radii of ≈3.5 Å. This makes the small 190 meV activation energy for Na^+ diffusion in $Na_2B_{10}H_{10}$ particularly noteworthy, since it is less than half that of $Na_2B_{12}H_{12}$ (410 meV).[16] Such a difference may be the result of the different natures of the diffusion saddle points inherent within the fcc and bcc structures, but may also signal a local geometric advantage that the less-spherical $B_{10}H_{10}^{2-}$ anions have over their more spherical relatives. In particular, within a cubic structure, one might expect each of the more-ellipsoidal $B_{10}H_{10}^{2-}$ anions to take up slightly less space in directions perpendicular to their long axes than the more spherical $B_{12}H_{12}^{2-}$ anions. On a local level, this would allow more free space between anions for cation diffusion. The QENS results are consistent with a locally ellipsoidal anion, by suggesting that each anion retains a particular orientation of its long axis over at least a nanosecond timescale.

Much needs to be done to provide a better understanding of the superionic properties of this new class of conducting materials. For example, since $Na_2B_{10}H_{10}$ possesses a much lower order–disorder phase-transition temperature than $Na_2B_{12}H_{12}$, one might think that the lighter-metal analogue, $Li_2B_{10}H_{10}$, would also possess a lower order–disorder phase-transition temperature than $Li_2B_{12}H_{12}$,[6,7] thus enhancing the stability of the disordered, fast-ion-conducting structure. Our $Li_2B_{10}H_{10}$ DSC measurements suggest the contrary. Rather, $Li_2B_{10}H_{10}$ appears to possess a slightly higher transition temperature than $Li_2B_{12}H_{12}$ does, leading to an unstable disordered structure, which makes it unsuitable as a solid-state, Li^+-conducting electrolyte. However, the addition of other anions or cations to $Li_2B_{10}H_{10}$ and to $Na_2B_{10}H_{10}$ may lead to hybrid materials displaying even lower transition temperatures than seen here for pure $Na_2B_{10}H_{10}$. We are currently pursuing such potentially favorable modifications.

For all these disordered materials, a more thorough understanding of the relationship of structural disorder and anion reorientational mobility to cation diffusion and conductivity will benefit from future first-principles molecular-dynamics calculations,[1,17,18] which may in turn lead to a more rational pathway to develop improved modified materials.

In conclusion, the discovery of very high superionic conductivity in $Na_2B_{10}H_{10}$ that persists to temperatures as low as 360 K is a marked improvement over $Na_2B_{12}H_{12}$ and other complex hydrides. Although hygroscopic, $Na_2B_{10}H_{10}$ remains air-stable at room temperature with no noticeable degradation in its diffraction pattern up to at least 500 K. DSC indicates that the compound decomposes/polymerizes with some mass loss of presumably H_2 at around 850 K. Preliminary cyclic voltammetry measurements indicate that ordered $Na_2B_{10}H_{10}$ is electrochemically stable up to at least 4 V at 353 K and disordered $Na_2B_{10}H_{10}$ up to at least 5 V at 393 K (see Figure S2 in the Supporting Information). Its favorable properties and high conductivity warrant a serious investigation of $Na_2B_{10}H_{10}$'s applicability to next-generation solid-state Na-ion battery technologies. Based on these results, successful future searches for related materials with even better cation conductivity properties may be enhanced by the inclusion of similar- or even larger-sized polyanions compared with $B_{10}H_{10}^{2-}$.

Experimental Section

Synthesis: ^{11}Boron-enriched $Na_2{}^{11}B_{10}H_{10}$ (and partially deuterated $Na_2{}^{11}B_{10}H_{10}$) was synthesized as follows: the triethylammonium salt $(Et_3NH)_2[^{11}B_{10}H_{10}]$ was synthesized via reaction of $^{11}B_{10}H_{14}$ (Katchem[19] and triethylamine in *para*-xylene at reflux. The crude product was recrystallized from water/EtOH and dried in vacuum (10 mTorr) at room temperature for 16 h. The $(Et_3NH)_2[^{11}B_{10}H_{10}]$ was then converted into the corresponding acid $(H_3O)_2[^{11}B_{10}H_{10}]$ by ion exchange using an Amberlite resin in H^+-form. Aqueous $Na_2{}^{11}B_{10}H_{10}$ was prepared by neutralization of $(H_3O)_2[^{11}B_{10}H_{10}]$ with 0.1 M NaOH until a pH value of 7 was reached. The solvent was removed on a rotary evaporator at 323 K. Unlabeled $Na_2B_{10}H_{10}$ was synthesized using a similar approach. The resulting hydrated materials were dried under vacuum at 433 K for 16 h. For the partially deuterated sample, a single exchange treatment was performed by dissolution and stirring for 3 h of 1 g of $Na_2{}^{11}B_{10}H_{10}$ in 20 mL of D_2O slightly acidified by adding 50 μL of a saturated solution of deuterochloric (DCl) acid in D_2O. The resulting dried sample had a D:H ratio of only 27:73 as determined from refinement of the 20 K NPD pattern, yet led to some reduction of the incoherent neutron scattering background from the lighter H isotope.

Measurement Details: DSC measurements were made with a Netzsch (STA 449 F1 Jupiter) TGA-DSC under He flow with Al sample pans. The neutron-scattering measurements were performed at the National Institute of Standards and Technology Center for Neutron Research. NPD patterns were measured on the BT-1 High-Resolution Powder Diffractometer using the Ge(311) monochromator at a neutron wavelength of 2.077 Å. Horizontal divergences of 60′, 20′, and 7′ of arc were used for the in-pile, monochromatic-beam, and diffracted-beam collimators, respectively. The sample was contained in a 6 mm-diameter V can inside a He closed-cycle refrigerator. FWSs were measured on the High-Flux Backscattering Spectrometer using 6.27 Å wavelength neutrons, with a resolution of 0.8 μeV FWHM. QENS spectra were collected at 270 K (resolution measurement) and 375 K on the Disk Chopper Spectrometer using 4.08 Å wavelength neutrons with a resolution of 79 μeV FWHM. ^{23}Na NMR measurements were performed on the pulse spectrometer described earlier[16] at the frequency $\omega/2\pi = 23$ MHz. The nuclear spin–lattice relaxation rates were measured

using the saturation–recovery method. NMR spectra were recorded by Fourier transforming the solid-echo signals. Ionic conductivities were determined in heating and cooling runs repeatedly in the temperature range between 303 K and 423 K by the AC complex-impedance method using an NF FRA5097 frequency response analyzer over a frequency range of 10 Hz to 10 MHz. All the measurements were performed under Ar. The powder sample was pressed into a pellet of 8 mm in diameter and 2 mm in thickness without sintering. The pellet density was about 1.17 g cm^{-3}, which is more than 95% of the density calculated from the lattice parameters. Au or Mo foils were used as electrodes and were mechanically fixed on both faces of the pellet. The resistances of the sample were obtained by least-square fittings of a single arc in the high-frequency range using equivalent circuits of a parallel combination of a resistance and a capacitance. At high temperature, since only a spike caused by the electrode contribution was observed, the resistance values were calculated from the intercept of the spike. The cross-section of the pelletized sample was examined by scanning electron microscopy (SEM) (JEOL JSM6009). Cyclic voltammetry measurements were conducted at scan rates of 5 mV s^{-1} using a potentiostat/galvanostat (Princeton VersaSTAT4) with a Mo disk as the working electrode and counter/reference electrodes of Na or Na–In at 353 K and 393 K, respectively. Finally, for all the figures, standard uncertainties are commensurate with the observed scatter in the data, if not explicitly designated by the vertical error bars.

Supporting Information

Supporting Information is available from the Wiley Online Library or from the author.

Acknowledgements

This work was performed, in part, in collaboration between members of IEA HIA Task 32-Hydrogen-based Energy Storage. The authors gratefully acknowledge support from DOE EERE through Grant Nos. DE-EE0002978 and DE-AC04–94AL85000; the Russian Foundation for Basic Research under Grant No. 12–03–00078; the U.S. Civilian Research & Development Foundation (CRDF Global) under Award No. RUP1–7076-EK-12; the National Science Foundation (NSF) under Cooperative Agreement No. OISE-9531011; the Integrated Materials Research Center for the Low-Carbon Society (LC-IMR), Tohoku University; the Advanced Low Carbon Technology Research and Development Program (ALCA) from the Japan Science and Technology Agency (JST); and JSPS KAKENHI under Grant Nos. 25220911 and 26820311. This work utilized facilities supported in part by the NSF under Agreement No. DMR-0944772. The authors also thank Dr. Nina Verdal for assistance with the QENS measurements.

Received: July 14, 2014
Revised: August 30, 2014
Published online: October 13, 2014

[1] A. Unemoto, M. Matsuo, S. Orimo, *Adv. Funct. Mater.* **2014**, *24*, 2267.
[2] M. Matsuo, Y. Nakamori, S. Orimo, H. Maekawa, H. Takamura, *Appl. Phys. Lett.* **2007**, *91*, 224103.
[3] H. Maekawa, M. Matsuo, H. Takamura, M. Ando, Y. Noda, T. Karahashi, S. Orimo, *J. Am. Chem. Soc.* **2009**, *131*, 894.
[4] M. Matsuo, S. Kuromoto, T. Sato, H. Oguchi, H. Takamura, S. Orimo, *Appl. Phys. Lett.* **2012**, *100*, 203904.
[5] A. Unemoto, S. Yasaku, G. Nogami, M. Tazawa, M. Taniguchi, M. Matsuo, T. Ikeshoji, S. Orimo, *Appl. Phys. Lett.* **2014**, *105*, 083901.
[6] M. Paskevicius, M. P. Pitt, D. H. Brown, D. A. Sheppard, S. Chumphongphan, C. E. Buckley, *Phys. Chem. Chem. Phys.* **2013**, *15*, 15825.
[7] N. Verdal, J.-H. Her, V. Stavila, A. V. Soloninin, O. A. Babanova, A. V. Skripov, T. J. Udovic, J. J. Rush, *J. Solid State Chem.* **2014**, *212*, 81.
[8] T. J. Udovic, M. Matsuo, A. Unemoto, N. Verdal, V. Stavila, A. V. Skripov, J. J. Rush, H. Takamura, S. Orimo, *Chem. Comm.* **2014**, *50*, 3750.
[9] K. B. Hueso, M. Armand, T. Rojo, *Energy Environ. Sci.* **2013**, *6*, 734.
[10] A. Hayashi, K. Noi, A. Sakuda, M. Tatsumisago, *Nat. Commun.* **2012**, *3*, 856.
[11] N. Tanibata, K. Noi, A. Hayashi, N. Kitamura, Y. Idemoto, M. Tatsumisago, *ChemElectroChem* **2014**, *1*, 1130.
[12] B. Bonnetot, H. Mongeot, A. Aboukhassib, F. Lefebvre, *Inorg. Chim. Acta* **1992**, *193*, 21.
[13] K. Hofmann, B. Albert, *Z. Kristallogr.* **2005**, *220*, 142.
[14] T. J. Udovic, N. Verdal, J. J. Rush, D. J. De Vries, M. R. Hartman, J. J. Vajo, A. F. Gross, A. V. Skripov, *J. Alloys Compd.* **2013**, *580*, S47.
[15] N. Verdal, T. J. Udovic, V. Stavila, W. S. Tang, J. J. Rush, A. V. Skripov, *J. Phys. Chem. C* **2014**, *118*, 17483.
[16] A. V. Skripov, O. A. Babanova, A. V. Soloninin, V. Stavila, N. Verdal, T. J. Udovic, J. J. Rush, *J. Phys. Chem. C* **2013**, *117*, 25961.
[17] B. C. Wood, N. Marzari, *Phys. Rev. Lett.* **2006**, *97*, 166401.
[18] J. S. G. Myrdal, D. Blanchard, D. Sveinbjörnsson, T. Vegge, *J. Phys. Chem C* **2013**, *117*, 9084.
[19] The mention of all commercial suppliers is for clarity and does not imply recommendation or endorsement by NIST.

ADVANCED MATERIALS

Supporting Information

for *Adv. Mater.*, DOI: 10.1002/adma.201403157

Exceptional Superionic Conductivity in Disordered Sodium Decahydro-*closo*-decaborate

*Terrence J. Udovic, Motoaki Matsuo, Wan Si Tang, Hui Wu, Vitalie Stavila, Alexei V. Soloninin, Roman V. Skoryunov, Olga A. Babanova, Alexander V. Skripov, John J. Rush, Atsushi Unemoto, Hitoshi Takamura, and Shin-ichi Orimo**

Supporting Information

Exceptional Superionic Conductivity in Disordered Sodium Decahydro-*closo*-decaborate

Terrence J. Udovic Motoaki Matsuo, Wan Si Tang, Hui Wu, Vitalie Stavila, Alexei V. Soloninin, Roman V. Skoryunov, Olga A. Babanova, Alexander V. Skripov, John J. Rush, Atsushi Unemoto, Hitoshi Takamura, and Shin-ichi Orimo**

NPD Results: The NPD patterns were analyzed by Rietveld refinement[1] using the GSAS package[2] assuming neutron scattering amplitudes of (3.63, 6.65, 6.67, and -3.74) fm for Na, ^{11}B, D, and H, respectively. A D:H ratio of 27:73 was determined from the low-temperature monoclinic structure[3] model fit to the data at 20 K, assuming a random isotopic distribution of D and H atoms. Wavelength errors were not included in the standard deviations of the unit cells; *i.e.*, the precisions reported in this paper for the structural parameters reflect the quality of the data and the corresponding refinement model, assuming a fixed neutron wavelength.

Table S1. Structure parameters of the high-*T* disordered phase (*Fm*-3*m*) of $Na_2{}^{11}B_{10}(H_{0.73}D_{0.27})_{10}$ at 410 K (*a*=9.8426(8) Å).

Atom	Site	x	y	z	U_{iso} (Å^2)	Occupancy
B1	24*e*	0.186	0	0	0.10	0.333
B2	96*k*	0.063	0.063	0.128	0.12	0.333
D1	24*e*	0.306	0	0	0.4	0.333
D2	96*k*	0.110	0.110	0.226	0.4	0.333
Na1	8c	0.25	0.25	0.25	0.15	0.58(1)
Na2	4*b*	0.5	0	0	0.4	0.28(3)
Na3	24*d*	0.25	0.25	0	0.3	0.09(1)

The center of the $B_{10}D_{10}^{2-}$ anion was fixed at the 4*a* site (0 0 0). B-D bond lengths were fixed at 1.173 Å. B-B bond lengths were fixed at those present in the low-*T* ordered $Na_2B_{10}H_{10}$ phase. R_{wp}=0.0123, R_p=0.0104, and χ^2=0.817. A neutron scattering amplitude of 0.73(-3.74) + 0.27(6.67) = -0.93 fm was used for the D1 and D2 atoms. Na positions were determined from a Fourier difference map, and Na site occupancies were refined using reasonable fixed U_{iso} values. It should be noted that the thermal factors and occupancies for Na were correlated. Changes in thermal factors affected the occupancies, but the variations in occupancies were not significant. The magnitudes of the Na1 (t), Na2 (o), and Na3 (i) site occupancies followed the same trend, i.e., occ(t) > occ(o) > occ(i), and the total number of Na atoms was basically around 8 per unit cell. This was also an indication of the correct structure model.

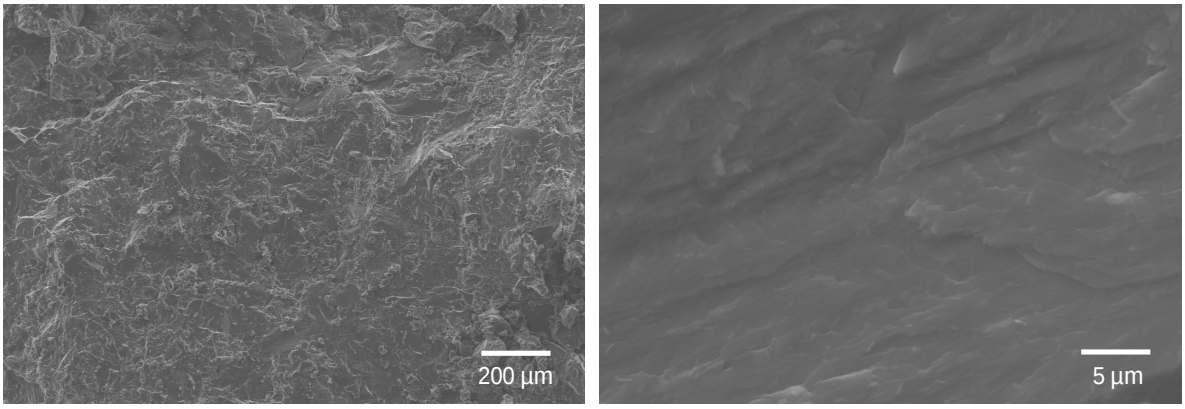

Figure S1. Cross-sectional SEM images of the pelletized $Na_2B_{10}H_{10}$ sample. As can be seen, intimate contacts among particles are achieved.

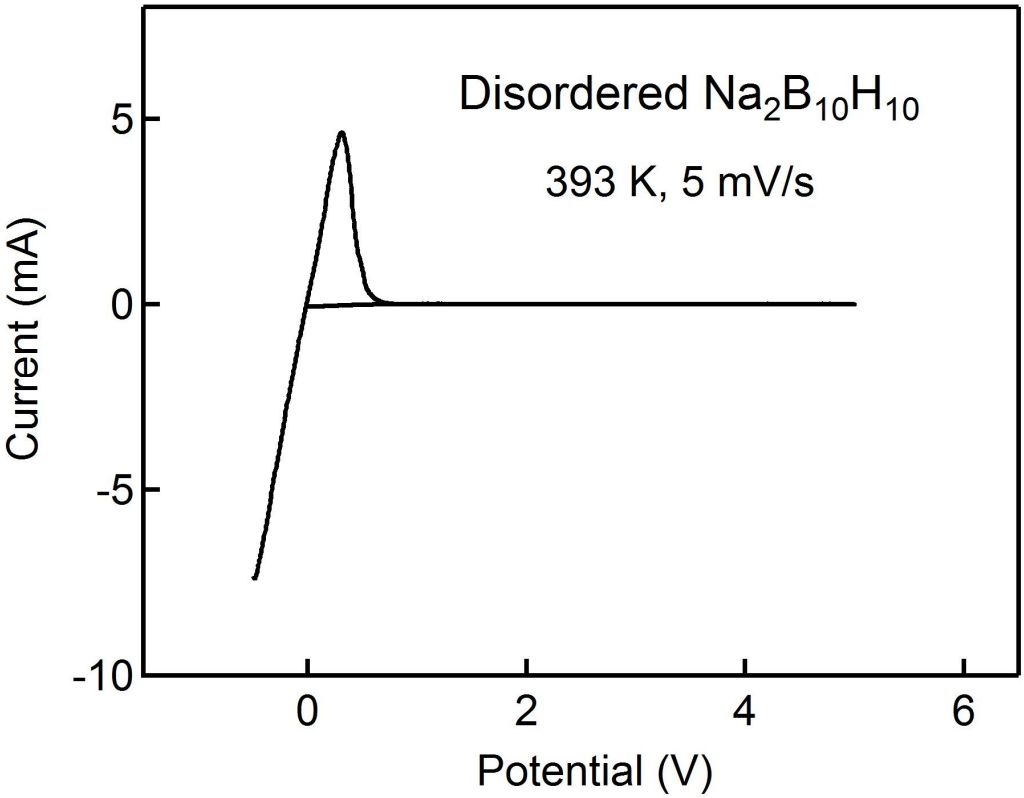

Figure S2. Cyclic voltammogram of disordered $Na_2B_{10}H_{10}$ at 393 K using Mo disk as the working electrode and a Na-In alloy as the counter/reference electrode at a scan rate of 5 mV s^{-1}.

[1] H. M. Rietveld, *J. Appl. Crystallogr.*, **1969**, *2*, 65.
[2] A. C. Larson, R. B. V. Dreele, *Los Alamos National Laboratory Report LAUR* 86-748, **1994**.
[3] K. Hofmann, B. Albert, *Z. Kristallogr.* **2005**, *220*, 142.